JPE 18-6-24

https://doi.org/10.6113/JPE.2018.18.6.1879
ISSN(Print): 1598-2092 / ISSN(Online): 2093-4718

Complex Vector Modeling and Series Decoupling Current Control Strategy of High-Power L/LCL Type Grid-Connected Converter Under Low Switching Frequency

Yingjie Wang[*,**], Lanyi Jiao[*], Bo Yang[*], Wenchao Wang[***], and Haiyuan Liu[†]

[*]School of Electrical and Power Engineering, China University of Mining and Technology, Xuzhou, China
[**]The State Key Laboratory of Heavy Duty AC Drive Electric Locomotive Systems Integration, Changsha, China
[***]Huizhou Power Supply Bureau, Huizhou, China
[†]School of Information and Control Engineering, China University of Mining and Technology, Xuzhou, China

Abstract

With power level of grid-connected converters rising, the switching frequency of the switching devices is commonly greatly reduced to improve its power capacity. However, this results in serious couplings of the *dq* current components, which leads to degradation of the static and dynamic performances of grid-connected converters and fluctuations of the reactive power in dynamic processes. In this paper, complex vector models under low switching frequency are established for an L/LCL grid-connected converter, and the relationship between the switching frequency and the coupling degree is analyzed. In addition, a series decoupling current control strategy is put forward. It is shown that the proposed control strategy can eliminate the couplings, improve the performances and have good robustness to parameter variations through static and dynamic characteristics analyses and a sensitivity analysis. Experimental and simulation results also verify the correctness of the theoretical analyses and the superiority of the proposed control strategy.

Key words: Complex vector, Decoupling current control strategy, Low switching frequency

I. INTRODUCTION

Grid-connected converters have advantages in terms of a sinusoidal output current, small harmonic content, bidirectional power flow and adjustable power factor. Since the connection hub is between the distributed power supply and the grid, it is widely used in renewable energy systems, power transmission systems, reactive power compensation systems, etc. With the expanding capacity of power demand, the power level of grid-connected converters has been rising. In order to increase the power capacity and to reduce losses, the switching frequency of the converter has to be greatly reduced [1]-[5]. For example, ABB ACS6000, which has an output power range from 3MVA to 36MVA, uses IGCT, and its switching frequency is around 500 Hz.

However, a reduction of the switching frequency increases the delay of the signal sampling and the PWM control in practical systems. Therefore, undesirable cross coupling is introduced in the d-q coordinates. The cross coupling affects the dynamic and static control performance of the grid-connected converter, making it difficult to design [6]-[9]. On the other hand, due to the coupling, when the active power command of the grid-connected converter changes, the reactive power fluctuates. Especially in high-power applications, the weak grid voltage is seriously affected by the reactive power.

At present, research on high performance control strategies

Manuscript received Mar. 5, 2018; accepted Aug. 29, 2018
Recommended for publication by Associate Editor T. Dragicevic.
[†]Corresponding Author: liu6340@126.com
Tel: +86-137-0520-6340,China University of Mining and Technology
[*]School of Electrical and Power Engineering, China University of Mining and Technology, China
[**]The State Key Laboratory of Heavy Duty AC Drive Electric Locomotive Systems Integration, China
[***]Huizhou Power Supply Bureau, China

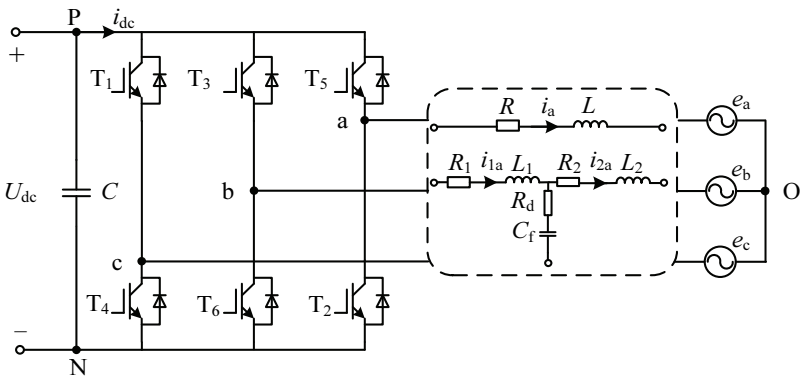

Fig. 1. Main circuit of a three-phase grid-connected converter.

for grid-connected converters under a low switching frequency is mainly divided into two aspects. On the one hand, the performance of the system is improved by adjusting the parameters of the regulator. In [10] and [11], a PI regulator is used in the d-q coordinate system, and the system is approximated as a second-order single input single output system with the cross coupling neglected. A set of parameter design methods is obtained. However, it should be pointed out that the approximation is not reasonable in [12]. A parameter design method based on the root locus of a multi input multi output system is given, which can completely eliminate the static coupling of the system. However, dynamic coupling still exists. On the other hand, the performance of the system is improved by a new control strategy. In [13], [14], a PR controller is used in the stationary coordinate system, which avoids the coupling problem. However, the dynamic performance of PR controller is inferior to that of a PI controller in the d-q coordinate system [15]. Model predictive control in stationary coordinate system has been proposed in [16]. However, the model prediction method has a problem since the switching frequency is not fixed. The relative gain matrix theory is used to analyze the coupling degree of the system, and a novel output feedback decoupling method is designed to decouple L type grid-connected converter systems under low switching frequency [17]. However, this method is difficult to use for converters with higher-order filters, such as LCL filters. Recently, in order to improve the ability to restrain high order harmonics and to reduce the filter volume and cost, LCL type grid-connected converters have become a trend. The decoupling control of LCL type grid-connected converters is carried out in [18]. However, it operates at a high switching frequency. At this point, the delay of signal sampling and PWM control have little influence on coupling. Therefore, it can be ignored. However, under a low switching frequency, there are 4 cross-coupling links in LCL type grid-connected converters, and there is no corresponding decoupling control method.

In 1954, W.V. Lyon first proposed the concept of complex vectors in the book "Transient Analysis of Alternating Current" [19]. The classical state matrix method and the complex vector analysis method have identical forms. The scalar of space vector, the real part and the imaginary part correspond to the corresponding matrix elements. The use of complex vectors for modeling, in addition to making the equations concise, reveals the internal electromagnetic relations of the system, which is a prominent advantage of complex vector analysis [20]-[22].

In this paper, an L/LCL type grid-connected converter model under a low switching frequency based on complex vector is established, and the coupling degrees at different switching frequencies are analyzed. Then based on the idea of zero pole cancellation, the series decoupling control strategies are proposed for the two converters. The frequency characteristics of the undecoupled and decoupled current control systems are compared, and the parameter sensitivity of the proposed strategies is analyzed. Finally, the correctness of the theoretical analysis and the proposed strategies are proved by experimental and simulation results.

II. L/LCL Type Grid-Connected Converter Model Under a Low Switching Frequency Based on Complex Vectors

A. L/LCL Type Grid-Connected Converter Model

The main circuit of a three-phase grid-connected converter is given in Fig. 1, and an L or LCL filter is usually used. T_1~T_6 denote the power switch tubes, C denotes the DC side capacitor, i_{dc} denotes the DC side current, U_{dc} denotes the DC side voltage, and e_a, e_b and e_c denote the phase voltages of the grid. In an L type grid-connected converter, L denotes the filter inductance, R includes the total equivalent resistance including the power loss equivalent resistance of the switch tubes and the parasitic resistance of the filter inductance, and i_a, i_b and i_c denote the three phase currents. In an LCL type grid-connected converter, L_1 denotes the converter side inductance, R_1 includes the total resistance including the power loss equivalent resistance of the switch tubes and the parasitic resistance of the inductance L_1, C_f denotes the filter capacitor, R_d denotes the damping resistor, L_2 denotes the grid

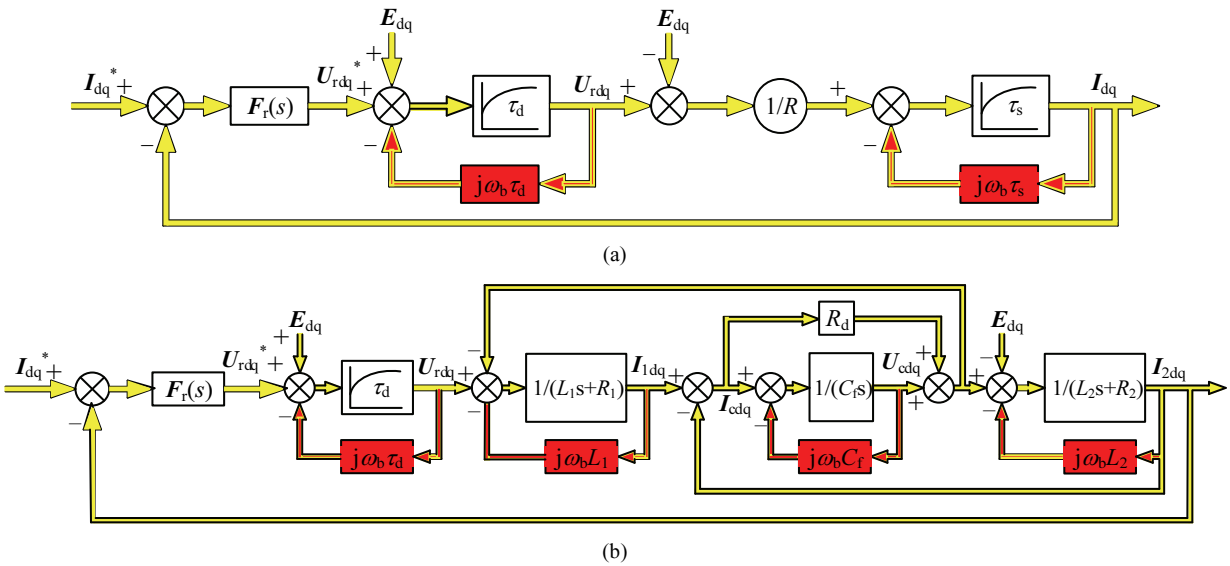

Fig. 2. Complex vector signal flow diagram of a current control system: (a) L type grid-connected converter; (b) LCL type grid-connected converter.

side inductance, and R_2 denotes the parasitic resistance of the inductance L_2. In addition, i_{1k} (k=a, b, c) denotes the converter side current, i_{2k} (k=a, b, c) denotes the grid side current, and i_{ck} (k=a, b, c) denotes the filter capacitor current.

According to Fig. 1, the AC side circuit equation of an L type grid-connected converter in the dq coordinate system is as follows.

$$\begin{bmatrix} e_d \\ e_q \end{bmatrix} = \begin{bmatrix} Lp+R & -\omega_b L \\ \omega_b L & Lp+R \end{bmatrix} \begin{bmatrix} i_d \\ i_q \end{bmatrix} + \begin{bmatrix} u_d \\ u_q \end{bmatrix} \tag{1}$$

Where e_d and e_q denote the d and q components of the phase voltages of the grid; u_d and u_q denote d and q components of converter side voltages; i_d, i_q denote the d and q components of the three phase currents; p denotes the differential operator; and ω_b denotes the angular frequency of the grid voltage.

According to (1), the circuit model of an L type grid-connected converter is reconstructed based on the concept of complex vector and transformed into the following complex transfer function:

$$\boldsymbol{F}_L(s) = \frac{\boldsymbol{I}_{dq}(s)}{\boldsymbol{E}_{dq}(s) - \boldsymbol{U}_{dq}(s)} = \frac{1}{R} \cdot \frac{1}{\tau_s(s+j\omega_b)+1} \tag{2}$$

Where τ_s=L/R.

Inevitably, there is a delay of the signal sampling and PWM control in practical systems, especially under a low switching frequency. This delay is so long that it cannot be ignored. Therefore, it is necessary to consider the influence of the delay. In general, the delay of signal sampling and PWM control includes one and a half switching period [7], [23], [24], namely, τ_d=$1.5/f_{sw}$. f_{sw} is the switching frequency of the grid-connected converter. If only the lower frequency range of the control system is focused on, the delay is equivalent to the first-order inertial link. Therefore, its complex vector transfer function is as follows.

$$\boldsymbol{F}_d(s) = \frac{\boldsymbol{U}_{rdq}(s)}{\boldsymbol{U}_{rdq}^{*}(s)} = \frac{1}{\tau_d(s+j\omega_b)+1} \tag{3}$$

Combining (2) and (3), the complex vector transfer function of the control object of the current control system is shown in (4), where S_j=s+jω_b. Thus, a complex vector signal flow chart of the current control system of L type grid-connected converters can be obtained, as shown in Fig. 2(a). $\boldsymbol{F}_r$(s) is the current controller. There are two complex factors j in the system, which indicates that there are two cross couplings. The cross couplings are caused by the differential action of the filter inductance and the first-order inertial link.

Similar to L type grid-connected converters, the complex vector transfer function of the control object of the current control system for LCL type grid-connected converters is obtained as (5). In (5), L_t=L_1+L_2 and R_t=R_1+R_2. A complex vector signal flow chart of the current control system of LCL type grid-connected converters is obtained, as shown in Fig. 2(b). From Fig. 2(b), it can be seen that there are four

$$\boldsymbol{F}_{m\_L}(s) = \frac{\boldsymbol{I}_{dq}(s)}{\boldsymbol{U}_{rdq}^{*}(s)} = \boldsymbol{F}_L(s) \cdot \boldsymbol{F}_d(s) = \frac{1}{R} \cdot \frac{1}{\tau_s(s+j\omega_b)+1} \cdot \frac{1}{\tau_d(s+j\omega_b)+1} = \frac{1}{R} \cdot \frac{1}{\tau_s S_j+1} \cdot \frac{1}{\tau_d S_j+1} \tag{4}$$

$$\boldsymbol{F}_{m\_LCL}(s) = \frac{\boldsymbol{I}_{2dq}(s)}{\boldsymbol{U}_{rdq}^{*}(s)} = \boldsymbol{F}_{LCL}(s)\boldsymbol{F}_d(s) = \frac{1}{\tau_d S_j+1} \cdot \frac{R_d C_f S_j+1}{C_f S_j(L_1 S_j+R_1)(L_2 S_j+R_2)+(L_t S_j+R_t)(R_d C_f S_j+1)} \tag{5}$$

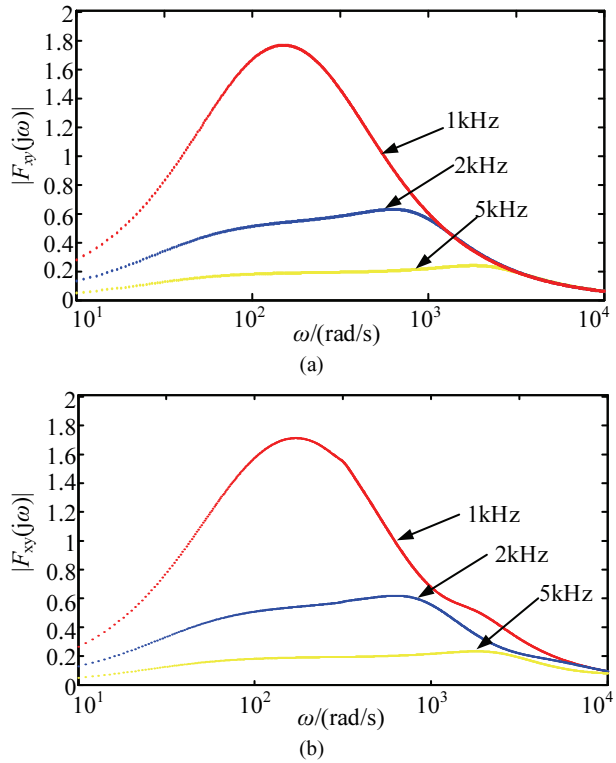

Fig. 3. Coupling function amplitude $|\boldsymbol{F}_{xy}(j\omega)|$ of an undecoupled closed-loop current control system: (a) L type grid-connected converter; (b) LCL type grid-connected converter.

complex factors, which indicates that there are four cross couplings. Three of them are introduced by L_1, L_2 and C_f in the LCL filter, and the last one is introduced by the first-order inertial link. Therefore, the couplings of LCL type grid-connected converters are more complex, which makes its control and design more difficult.

B. Coupling Analysis

From the above modeling process, it is known that the cross couplings between the variables corresponds to the imaginary part. In order to intuitively analyze the coupling degree of the system, the coupling function $\boldsymbol{F}_{xy}(j\omega)$ is defined as:

$$\boldsymbol{F}_{xy}(j\omega)=\frac{\mathrm{Im}\{\boldsymbol{F}(j\omega)\}}{\mathrm{Re}\{\boldsymbol{F}(j\omega)\}} \tag{6}$$

If the current control system is undecoupled and a PI regulator is used, the current controller $\boldsymbol{F}_r(s)$ is as follows.

$$\boldsymbol{F}_r(s)=\frac{K_p(\tau_r s+1)}{\tau_r s} \tag{7}$$

The coupling function amplitude $|\boldsymbol{F}_{xy}(j\omega)|$ of the undecoupled closed-loop current control system can be obtained by (4)-(7), as shown in Fig. 3. Fig. 3(a) shows the coupling curves of an L type grid-connected converter. Fig. 3(b) shows the coupling curves of an LCL type grid-connected converter. It can be seen that the coupling degree

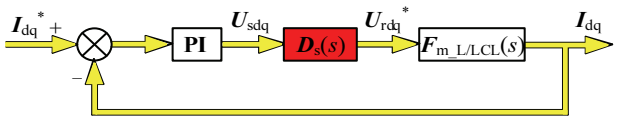

Fig. 4. Complex vector signal flow diagram of a series decoupling current closed-loop control system.

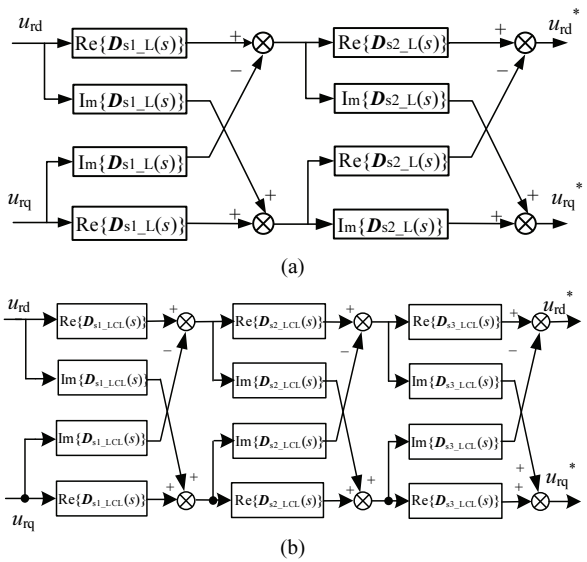

Fig. 5. Diagram of a series decoupling unit: (a) L type grid-connected converter; (b) LCL type grid-connected converter.

of the current control system increases gradually with a decrease of the switching frequency, and that the coupling degree is most serious near the fundamental frequency. In order to solve this problem, a series decoupling strategy based on a complex vector under a low switching frequency is proposed in the following section.

III. Series Decoupling Strategy Based on a Complex Vector Under a Low Switching Frequency

From (7), it is shown that there are no complex zeros in the PI regulator to eliminate the complex poles of the control object. In this paper, a series decoupling strategy is used to offset the complex poles. A complex vector signal flow diagram of a series decoupling closed-loop current control system is shown in Fig. 4. $\boldsymbol{D}_s(s)$ is a series decoupling unit. In theory, the decoupling unit can be designed on the bases of any target system. Only these couplings are eliminated by the proposed strategy in order to retain its main channel characteristics.

A. Decoupling Strategy of L Type Grid-connected Converters

According to (4), the series decoupling unit, which can retain the main channel characteristic, is required as:

$$\boldsymbol{D}_{s\_L}(s)=\frac{(\tau_s S_j+1)(\tau_d S_j+1)}{(\tau_s s+1)(\tau_d s+1)} \tag{8}$$

In (9), in order to facilitate implementation, $\boldsymbol{D}_{s\_L}(s)$ is decomposed into $\boldsymbol{D}_{s1}(s)$ and $\boldsymbol{D}_{s2}(s)$. In this case, $\boldsymbol{D}_{s1}(s)$ is the decoupling unit for delay, and $\boldsymbol{D}_{s2}(s)$ is the decoupling unit for the grid-connected converter-controlled object. In (10), the decoupling units are shown and they are separated into an actual part and an imaginary part. In order to preserve the characteristic of the main channel, the real part is written as "1+", and the block diagram is shown in Fig. 5(a).

$$\boldsymbol{D}_{s\_L}(s)=\boldsymbol{D}_{s1\_L}(s)\boldsymbol{D}_{s2\_L}(s) \tag{9}$$

$$\begin{cases}\boldsymbol{D}_{s1\_L}(s)=1+\mathrm{j}\dfrac{\omega_b\tau_d}{\tau_d s+1}\\ \boldsymbol{D}_{s2\_L}(s)=1+\mathrm{j}\dfrac{\omega_b\tau_s}{\tau_s s+1}\end{cases} \tag{10}$$

Then the complex vector transfer function of the open-loop current control system of an L type grid-connected converter is decoupled as:

$$\boldsymbol{F}_{oc\_s\_L}(s)=\frac{K_p(\tau_r s+1)}{R\tau_r s(\tau_d s+1)(\tau_s s+1)} \tag{11}$$

B. Decoupling Strategy of LCL Type Grid-connected Converters

Similar to an L type grid-connected converter, the series decoupling unit for an LCL type grid-connected converter is shown in (13). In (12), $\boldsymbol{D}(s)$ is decomposed into $\boldsymbol{D}_{s1}(s)$, $\boldsymbol{D}_{s2}(s)$ and $\boldsymbol{D}_{s3}(s)$. In this case, $\boldsymbol{D}_{s1}(s)$ is the decoupling unit for the delay, $\boldsymbol{D}_{s2}(s)$ is the decoupling unit for the complex zero of the grid-connected converter-controlled object, and $\boldsymbol{D}_{s3}(s)$ is the decoupling unit for the complex pole of the grid-connected converter-controlled object. The decoupling units are shown in (14). In order to retain the characteristic of the main channel, the real part is written as "1+", and the block diagram is shown in Fig. 5(b).

$$\boldsymbol{D}_s(s)=\boldsymbol{D}_{s1}(s)\boldsymbol{D}_{s2}(s)\boldsymbol{D}_{s3}(s) \tag{12}$$

After decoupling, the complex vector transfer function of the open-loop current control system of an LCL type grid-connected converter is shown in (15).

IV. Comparison Analysis of Undecoupled and Series Decoupled Current Control Systems

In this paper, the stability, dynamic performance and parameter sensitivity of undecoupled and series decoupled systems are analyzed and compared under the condition that the main circuit parameters are constants. Under a low switching frequency, the dynamic performance of a traditional feed-forward decoupled system is worse than that of an undecoupled system [17]. Therefore, in this paper, a detailed comparison was made between an undecoupled system and a system with the proposed series decoupling strategy.

A. Analysis of the Frequency Domain and the Time Domain

In Figs. 6(a)-(d), the root loci of undecoupled systems and series decoupled systems of L and LCL type grid-connected converters are given at f_{sw}=1 kHz. It can be seen that for small values of K_p, some of the poles of the undecoupled current control systems are in the right half-plane (RHP). However, the dominant poles of the series decoupled current control systems are always in the left half-plane (LHP). This means that the series decoupling strategy increases stability. From Figs. 6(c) and 6(d), two poles move towards the RHP with K_p increasing. This is due to the fact that the resonance suppression for the LCL filter deteriorates with K_p increasing, rather than the coupling.

In Figs. 6(e) and 6(f), the step responses of undecoupled systems and series decoupled systems of L and LCL type grid-connected converters are given at f_{sw}=1kHz. The *d* axis current component of the undecoupled system influences the *q* axis component through the coupling channel, which leads to a larger fluctuation of the *q* axis current component. It needs to undergo a mutation process to return to the original steady state value. Although there is no static coupling, the undecoupled system needs a longer regulation time. As a result, even if a grid-connected converter is in unit power factor operation, when the active current is mutated, the reactive current is seriously affected through the coupling channel. Fluctuations of the reactive current inevitably affect

$$\boldsymbol{D}_s(s)=\frac{\boldsymbol{F}_{oc\_LCL}(s)}{\boldsymbol{F}_{m\_LCL}(s)}=\frac{\tau_d S_j+1}{\tau_d s+1}\bullet\frac{R_dC_fs+1}{R_dC_fS_j+1}\bullet\frac{C_fS_j\left(L_1S_j+R_1\right)\left(L_2S_j+R_2\right)+\left(L_tS_j+R_t\right)\left(R_dC_fS_j+1\right)}{C_fs\left(L_1s+R_1\right)\left(L_2s+R_2\right)+\left(L_ts+R_t\right)\left(R_dC_fs+1\right)} \tag{13}$$

$$\begin{cases}\boldsymbol{D}_{s1}(s)=1+\mathrm{j}\dfrac{\omega_b\tau_d}{\tau_d s+1}\\ \boldsymbol{D}_{s2}(s)=1-\dfrac{\omega_b^2R_d^2C_f^2}{\left(R_dC_fs+1\right)^2+\omega_b^2R_d^2C_f^2}-\mathrm{j}\dfrac{\omega_bR_dC_f\left(R_dC_fs+1\right)}{\left(R_dC_fs+1\right)^2+\omega_b^2R_d^2C_f^2}\\ \boldsymbol{D}_{s3}(s)=1-\dfrac{3\omega_b^2L_1L_2C_fs+\omega_b^2C_f\left(L_1R_2+L_2R_1\right)}{C_fs\left(L_1s+R_1\right)\left(L_2s+R_2\right)+\left(L_ts+R_t\right)\left(R_dC_fs+1\right)}+\mathrm{j}\omega_bC_f\dfrac{\left(3L_1L_2+2L_1R_2+2L_2R_1\right)s+R_1R_2-L_1L_2}{C_fs\left(L_1s+R_1\right)\left(L_2s+R_2\right)+\left(L_ts+R_t\right)\left(R_dC_fs+1\right)}\end{cases} \tag{14}$$

$$\boldsymbol{F}_{oc\_s}(s)=\boldsymbol{F}_r(s)\boldsymbol{F}_s(s)=K_p\bullet\frac{\tau_rs+1}{\tau_rs}\bullet\frac{1}{\tau_ds+1}\bullet\frac{R_dC_fs+1}{C_fs\left(L_1s+R_1\right)\left(L_2s+R_2\right)+\left(L_ts+R_t\right)\left(R_dC_fs+1\right)} \tag{15}$$

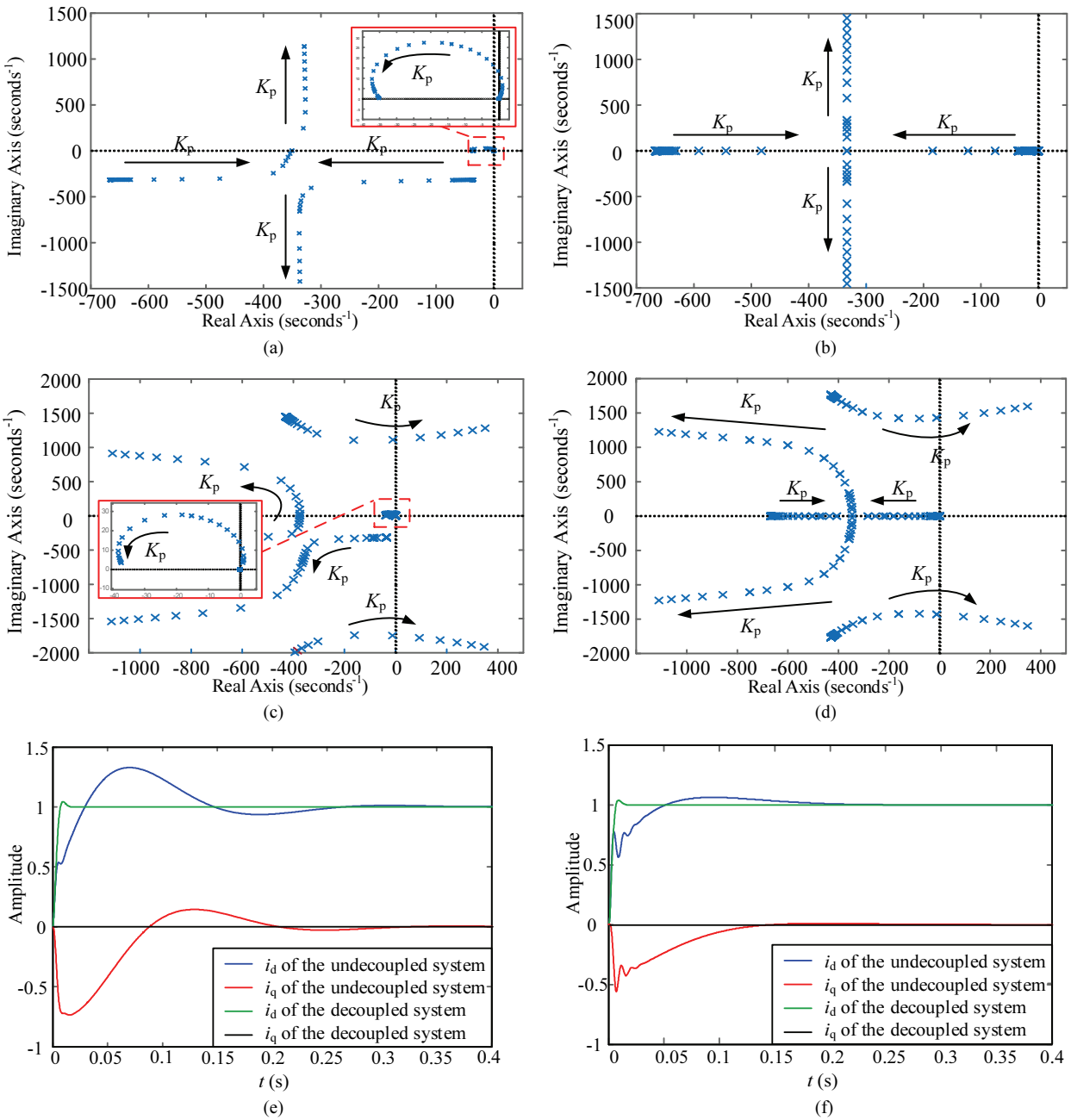

Fig. 6. Root loci and time domain curves of an undecoupled system and a series decoupled current control system: (a) Root locus of L type with the undecoupling method; (b) Root locus of L type with the series decoupling method; (c) Root locus of LCL type with the undecoupling method; (d) Root locus of LCL type with the series decoupling method; (e) Step response of an L type grid-connected converter; (f) Step response of an LCL type grid-connected converter.

the grid voltage. When it occurs at a high-power grid-connected converter, the grid voltage is greatly impacted.

When the *d* axis current component is fed into the unit step signal, a series decoupled system has a smaller overshoot, shorter rise time and shorter time to reach its steady state. The *d* axis and *q* axis current components do not affect each other and couplings do not exist.

B. Parameter Sensitivity Analysis

Since the series decoupling current control strategy proposed in this paper is designed based on the principle of zero pole cancellation, the decoupling performance is influenced by the system parameters that determine the positions of the zero and poles. The parameters in an actual system may be changed by factors such as current, temperature, etc. In order to analyze the parameter sensitivity of the proposed strategy, the open-loop frequency characteristics of an LCL type grid-connected converter is shown in Fig. 7. Here, the filter parameters L_1, L_2 and C_f are changed when the other system parameters are unchanged. In addition, L_1, L_2 and C_f vary from -30% to +30%.

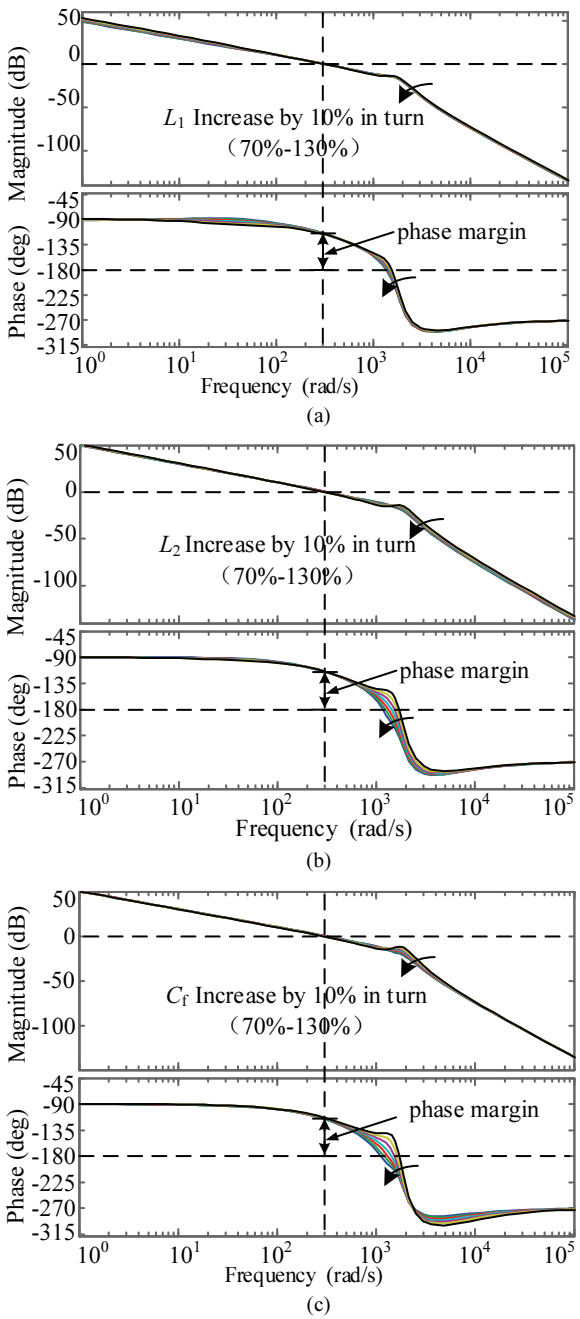

Fig. 7. Frequency characteristics of the series decoupled system at 1kHz for parameter variations for: (a) L_1 ±30%; (b) L_2 ±30%; (c) C_f ±30%.

It can be seen that the proposed decoupling method has a good robustness.

V. Experimental and Simulation Results

A. Experimental Results

A laboratory setup of an L/LCL type grid-connected converter, shown in Fig. 8, has been built to verify the proposed series decoupling strategy and to compare its performance with the traditional undecoupled strategy at a low switching frequency. A high-performance NI cRIO-9024 of National Instruments Company is used as the core controller, IGBTs from INFINEON Company are used, and the driving circuit for the IGBTs is designed on the basis of a dual SCALE driver 2SD315A from CONCEPT Company. The experimental parameters are shown in Table I.

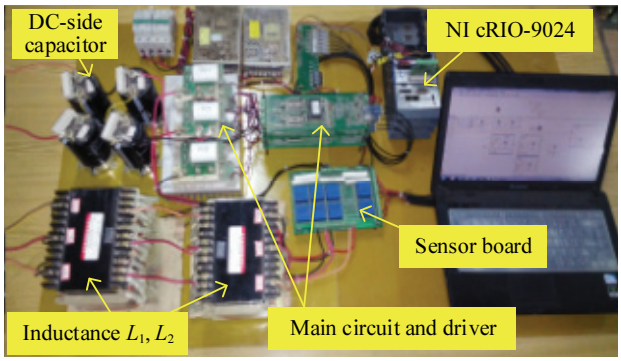

Fig. 8. Laboratory setup of an L/LCL type grid-connected converter.

TABLE I
Experimental Parameters

Symbol	Description	Value
E_{ab}, E_{bc}, E_{ca}	The grid line voltages(rms)	50V
L_1	Converter side inductance	3mH
L_2	Grid side inductance	3mH
C_f	Filter capacitor	100μF
R_d	Damping resistor	1Ω
f_b	Grid frequency	50Hz
f_{sw}	Switching frequency	1kHz
U_{dc}	DC side voltage	120V
$L = L_1 + L_2$	Inductance	6mH

In the experiment, the grid-connected converters operate in the inverter state. The reactive current is given zero when two grid-connected converts are operating at a unity power factor. The d and q components of the grid-side current are output to the oscilloscope through the DAC module the NI 9263. The whole control system framework of the two grid converters can be seen in Fig. 1.

In Fig. 9, experimental waveforms of the undecoupled system and the proposed decoupled system for an L type grid connected converter at f_{sw} = 1 kHz are given. Waveforms of the undecoupled system are in Figs. 9(a), 9(b) and 9(c). Waveforms of the decoupled system are in Figs. 9(d), 9(e) and 9(f). From Figs. 9(a) and 9(d), the waveforms of the DC voltage U_{dc} and the d and q components of the grid-side current are given when the d component mutates from 5A to 10A. The mutation makes the response speed slower, the overshoot bigger, and the fluctuation on i_q larger when the undecoupled method is employed. When compared with the undecoupled system, the series decoupled system has good control performance. The response speed is faster. The

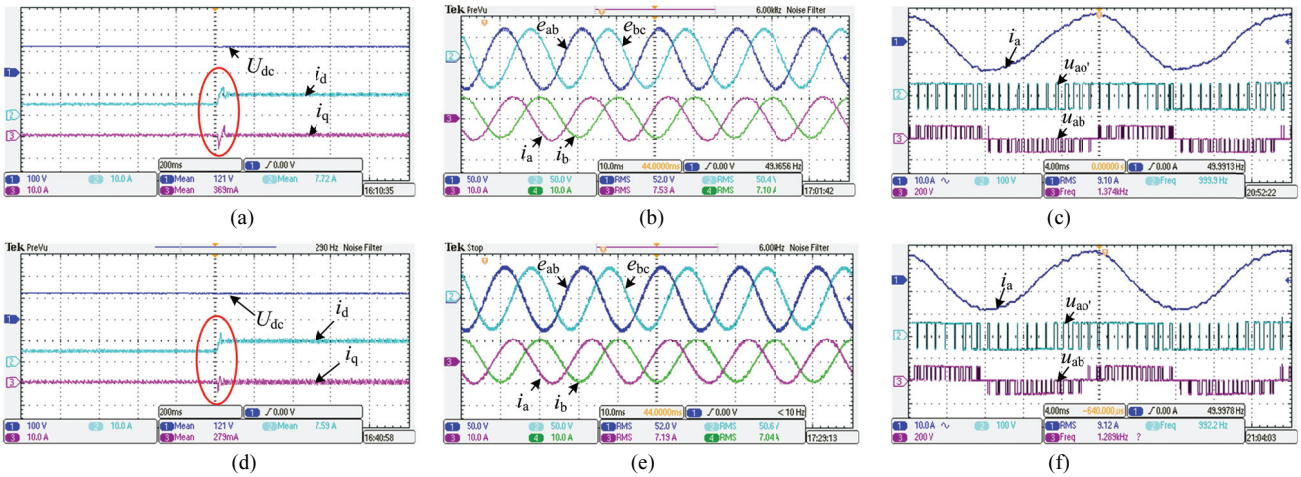

Fig. 9. Experimental waveforms with different control methods for a L type grid-connected converter at f_{sw} = 1 kHz: (a), (b), (c) with the undecoupling method; (d), (e), (f) with the proposed decoupling method.

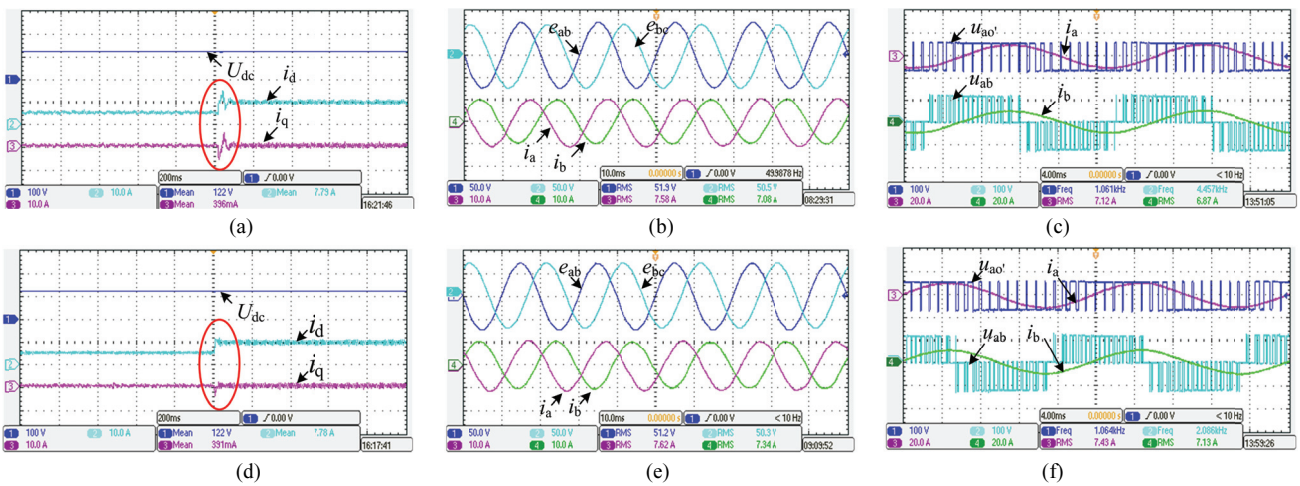

Fig. 10. Experimental waveforms with different control methods for an LCL type grid-connected converter at f_{sw} = 1 kHz: (a), (b), (c) with the undecoupling method; (d), (e), (f) with the proposed decoupling method.

overshoot is smaller, and the fluctuation on the i_q component can be weakened to a certain extent.

In Fig. 10, experimental waveforms of the undecoupled system and decoupled system for an LCL type grid connected converter at f_{sw} = 1 kHz are given. Waveforms of the undecoupled system are shown in Figs. 10(a), 10(b) and 10(c); and waveforms of the proposed decoupled system are shown in Figs. 10(d), 10(e) and 10(f). The experimental results are similar to the results shown in Fig. 9.

From Fig. 9 and Fig. 10, the experimental results show that the proposed series decoupling strategy can effectively eliminate the dynamic couplings of the system and improve the control performance of the system.

B. Simulation Results

The current control strategy proposed in this paper is designed for high-power converters. Therefore, the decoupling phenomenon is more obvious in high-power converters. Due to limited laboratory conditions, experimental verification of high-power converters cannot be performed. For further verification, a series of simulations were done, and the power level of the converter is 2MW. The simulation waveforms are shown in Fig. 11. It can be seen that the coupling problem of the high-power converter is obvious. In addition, the proposed decoupling method reduces the fluctuation of i_q from 1083A down to 286A. It significantly reduces the fluctuation on i_q.

Here, a statistics table is made based on the difference of Δi_d^*. In this case, Δi_d^* denotes the change of the set value of i_d. In addition, Δi_q denotes the fluctuation on i_q. In Fig. 12(a), it is found that the greater Δi_d^*, the greater the fluctuation on i_q. In this case, the superiority of the proposed control strategy can be reflected. The fluctuation on i_q causes the reactive power to fluctuate, as shown in Fig. 12(b). Q denotes the transient reactive power of this converter. In addition, the proposed strategy can significantly improve this.

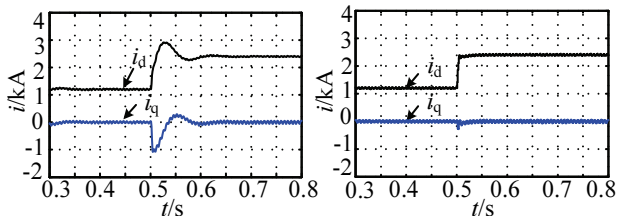

Fig. 11. Simulation waveforms with different control methods for an LCL type grid-connected converter at f_{sw} = 1 kHz: (a) With the undecoupling method; (b) With the proposed decoupling method.

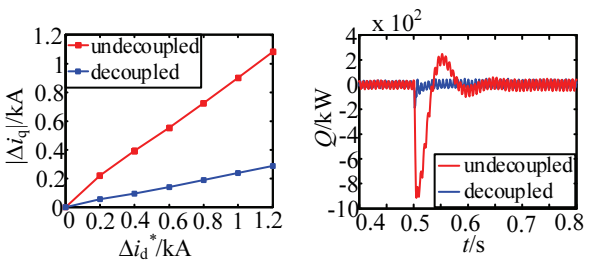

Fig. 12. Simulation results of an LCL type grid-connected converter at f_{sw} = 1 kHz: (a) Statistics of the fluctuation on i_q based on the difference of Δi_d^*; (b) Fluctuation on the reactive power when Δi_d^*=1.2kA.

VI. Conclusions

In this paper, the complex vector is used to model L/LCL type grid-connected converters. The modeling method has the characteristics of simple equation, graphic expression and is easy to understand. In addition, it can simplify the system expression and decoupling process. By analyzing the coupling degree of two kinds of undecoupled systems, it is found that the coupling degree increases with a decrease of the switching frequency. For this reason, two series decoupling current control strategies based on the complex vector for L and LCL type grid-connected converters is proposed in this paper. The *dq* components of the grid-side currents are decoupled in series. The time domain and frequency domain analyses show that the proposed strategies can effectively suppress the current cross coupling phenomenon caused by a low switching frequency. It can also achieve better dynamic performance and a greater stability margin. The sensitivity analysis shows that the proposed strategies has good robustness when the system parameters change greatly. Finally, the experimental and simulation results verify the correctness of the theoretical analyses and the superiorities of the proposed control strategy.

Under a unit power factor, the proposed decoupling method can realize power decoupling, especially in the dynamic process. It has practical value for the independent control and flexible regulation of the reactive power and active power of microgrids.

Acknowledgment

The authors gratefully acknowledge the support provided by the Fundamental Research Funds for the Central Universities (2017XKQY029).

References

[1] L. G. Franquelo, J. I. Leon, and E. Dominguez, "New trends and topologies for high power industrial applications: The multilevel converters solution," *International Conference on Power Engineering, Energy and Electrical Drives*, pp. 1-6, 2009.

[2] K. Ma and F. Blaabjerg, "Thermal optimised modulation methods of three-level neutral-point-clamped inverter for 10 MW wind turbines under low-voltage ride through," *IET Power Electron.*, Vol. 5, No. 6, pp. 920-927, Jul. 2012.

[3] J. A. Pontt, J. R. Rodriguez, A. Liendo, P. Newman, J. Holtz, and J. M. S. Martin, "Network-friendly low-switching-frequency multipulse high-power three- level PWM rectifier," *IEEE Trans. Ind. Electron.*, Vol. 56, No. 4, pp. 1254-1262, Apr. 2009.

[4] J. Holtz and X. Qi, "Optimal control of medium-voltage drives – An overview," *IEEE Trans. Ind. Electron.*, Vol. 60, No. 12, pp. 5472-5481, Dec. 2013.

[5] A. G. Siemens, "Power semiconductors: For medium voltage converters – An overview," *European Conference on Power Electronics and Applications*, pp. 121-134, 2009.

[6] H. Kim, M. W. Degner, J. M. Guerrero, F. Briz, and R. D. Lorenz, "Discrete-time current regulator design for AC machine drives," *IEEE Trans. Ind. Appl.*, Vol. 46, No. 4, pp. 1425-1435, Jul./Aug. 2010.

[7] J. Holtz, J. Quan, J. Pontt, and J. Rodriguez, "Design of fast and robust current regulators for high-power drives based on complex state variables," *IEEE Trans. Ind. Appl.,* Vol. 40, No. 5, pp. 1388-1397, Sep./Oct. 2004.

[8] J. S. Yim, S. K. Sul, B. H. Bae, N. R. Patel, and S. Hiti, "Modified current control schemes for high-performance permanent-magnet ac drives with low sampling to operating frequency ratio," *IEEE Trans. Ind. Appl.,* Vol. 45, No. 2, pp. 763-771, Mar./Apr. 2009.

[9] M. Ke, M. Liserre, and F. Blaabjerg, "Operating and loading conditions of a three-level neutral-point-clamped wind power converter under various grid faults," *IEEE Trans. Ind. Appl.*, Vol. 50, No. 1, pp. 520-530, Jan./Feb. 2014.

[10] A. G. Yepes, A. Vidal, J. Malvar, O. Lopez, and J. Doval-Gandoy, "Tuning method aimed at optimized settling time and overshoot for synchronous proportional-integral current control in electric machines," *IEEE Trans. Power Electron.,* Vol. 29, No. 6, pp. 3041-3054, Jun. 2014.

[11] D. G. Holmes, T. A. Lipo, B. P. Mcgrath, and W. Y. Kong, "Optimized design of stationary frame three phase AC current regulators," *IEEE Trans. Power Electron.*, Vol. 24, No. 11, pp. 2417-2426, Nov. 2009.

[12] F. D. Freijedo, A. Vidal, A. G. Yepes, J. M. Guerrero, Ó. López, J. Malvar, and J. Doval-Gandoy, "Tuning of synchronous-frame PI current controllers in grid-connected converters operating at a low sampling rate by mimo root locus," *IEEE Trans. Ind. Electron.*, Vol. 62, No. 8, pp. 5006-5017, Aug. 2015.

[13] K. Tan, Q. Ge, Z. Yin, L. Tan, C. Liu, and Y Li, "The optimized strategy for input current harmonic of low switching frequency PWM rectifier," *2010 5th IEEE Conference on Industrial Electronics and Applications*, pp. 1057-1061, 2010.
[14] A. Ghoshal and V. John, "Active damping of LCL filter at low switching to resonance frequency ratio," *IET Power Electron.*, Vol. 8, No. 4, pp. 574-582, Apr. 2015.
[15] J. G. Hwang, P. W. Lehn, and M. Winkelnkemper, "A generalized class of stationary frame-current controllers for grid-connected AC-DC converters," *IEEE Trans. Power Del.*, Vol. 25, No. 4, pp. 2742-2751, Oct. 2010.
[16] S. Kouro, P. Cortes, R. Vargas, U. Ammann, and J. Rodriguez, "Model predictive control – A simple and powerful method to control power converters," *IEEE Trans. Ind. Electron.*, Vol. 56, No. 6, pp. 1826-1838, Jun. 2009.
[17] Y. Wang, W. Wang, C. Wang, and X. Wu, "Coupling analysis on current control at low switching frequency for the three-phase PWM converter based on RGA and a novel output feedback decoupling method," *IEEE Trans. Ind. Electron.,* Vol. 63, No. 11, pp. 6684-6694, Nov. 2016.
[18] S. A. Khajehoddin, M. Karimi-Ghartemani, P. K. Jain, and A. Bakhshai, "A control design approach for three-phase grid-connected renewable energy resources," *IEEE Trans. Sustain. Energy*, Vol. 2, No. 4, pp. 423- 432, Oct. 2011.
[19] W. Lyon, Transient Analysis of Alternating-current Machinery, Wiley, 1954.
[20] J. Holtz, "The representation of AC machine dynamics by complex signal flow graphs," *IEEE Trans. Ind. Electron.*, Vol. 42, No. 3, pp. 263-271, Jun. 1995.
[21] K. Dai, P. Liu, J. Xiong, and J. Chen, "Comparative study on current control for three-phase SVPWM voltage-source converter in synchronous rotating frame using complex vector method," *IEEE Power Electronics Specialist Conference*, Vol. 2, pp. 695-700, 2003.
[22] J. Holtz and N. Oikonomou, "Estimation of the fundamental current in low-switching-frequency high dynamic medium-voltage drives," *IEEE Trans. Ind. Appl.,* Vol. 44, No. 5, pp. 1597-1605, Sep./Oct. 2008.
[23] J. S. Yim, S. K. Sul, B. H. Bae, N. R. Patel, and S. Hiti, "Modified current control schemes for high-performance permanent-magnet AC drives with low sampling to operating frequency ratio," *IEEE Trans. Ind. Appl.*, Vol. 45, No. 2, pp. 763-771, Mar./Apr. 2009.
[24] D. G. Holmes, T. A. Lipo, B. P. McGrath, and W. Y. Kong, "Optimized design of stationary frame three phase AC current regulators," *IEEE Trans. Power Electron.*, Vol. 24, No. 11, pp. 2417-2426, Nov. 2009.

Yingjie Wang was born in Zhejiang, China, in 1979. He received his B.S. degree in Mechanical Engineering from Central South University, Changsha, China, in 2001; and his Ph.D. degree in Electrical Engineering from the China University of Mining and Technology, Xuzhou, China, in 2012. He is presently working as an Associate Professor in School of Electrical and Power Engineering, China University of Mining and Technology. His current research interests include power quality, microgrids and medium-voltage ac drives.

Lanyi Jiao was born in Shanxi, China, in 1994. He received his B.S. degree in Electrical Engineering from Shanxi Agricultural University, Jinzhong, China, in 2016. He is presently working towards his M.S. degree in Electrical Engineering at the China University of Mining and Technology, Xuzhou, China. His current research interests include traction system stability, renewable energy generation systems and microgrids.

Bo Yang was born in Jiangsu, China, in 1994. He received his B.S. degree in Electrical Engineering from the China University of Mining and Technology, Xuzhou, China, in 2017, where he is presently working towards his M.S. degree in Electrical Engineering. His current research interests include MMC HVDC and microgrids.

Wenchao Wang was born in Guangdong, China, in 1991. He received his B.S. and M.S. degrees from the School of Electrical and Power Engineering, China University of Mining and Technology, Xuzhou, China, in 2014 and 2017, respectively. After graduating, he joined Huizhou Power Supply Bureau, Huizhou, China. His current research interests include power quality, renewable energy generation systems and microgrids.

Haiyuan Liu was born in Zhejiang, China, in 1980. She received her B.S. degree from Sichuan Normal University, Chengdu, China, in 2001; and her M.S. degree from the China University of Mining and Technology, Xuzhou, China, in 2006, where she is presently working towards her Ph.D. degree. She is also working a Lecturer in the School of Mathematics, China University of Mining and Technology. Her current research interests include intelligent control theory and applications.